Earth and Planetary Science Letters 301 (2011) 222–230

Contents lists available at ScienceDirect

Earth and Planetary Science Letters

journal homepage: www.elsevier.com/locate/epsl

Coupled silicon–oxygen isotope fractionation traces Archaean silicification

K. Abraham [a,b,*], A. Hofmann [c], S.F. Foley [a], D. Cardinal [b,d], C. Harris [e], M.G. Barth [a], L. André [b]

[a] Institut für Geowissenschaften, Universität Mainz, Becherweg 21, D-55099 Mainz, Germany
[b] Section de Minéralogie—Pétrographie—Géochimie, Musée Royal de l'Afrique Centrale, Leuvensesteenweg 13, B-3080 Tervuren, Belgium
[c] Department of Geology, University of Johannesburg, South Africa
[d] LOCEAN, Université Pierre et Marie Curie, 4 Place Jussieu, F-75005 Paris, France
[e] Department of Geological Sciences, University of Cape Town, Rondebosch 7701, South Africa

ARTICLE INFO

Article history:
Received 29 March 2010
Received in revised form 29 October 2010
Accepted 1 November 2010
Available online 8 December 2010

Editor: R.W. Carlson

Keywords:
Si isotopes
O isotopes
Barberton Greenstone Belt
silicification
two-step process

ABSTRACT

Silica alteration zones and cherts are a conspicuous feature of Archaean greenstone belts worldwide and provide evidence of extensive mobilisation of silica in the marine environment of the early Earth. In order to understand the process(es) of silicification we measured the silicon and oxygen isotope composition of sections of variably silicified basalts and overlying bedded cherts from the Theespruit, Hooggenoeg and Kromberg Formations of the Barberton Greenstone Belt, South Africa.

The δ^{30}Si and δ^{18}O values of bulk rock increase with increasing amount of silicification from unsilicified basalts ($-0.64‰<\delta^{30}Si<-0.01‰$ and $+8.6‰<\delta^{18}O<+11.9‰$) to silicified basalts (δ^{30}Si and δ^{18}O values as high as $+0.81‰$ and $+15.6‰$, respectively). Cherts generally have positive isotope ratios ($+0.21‰<\delta^{30}Si<+1.05‰$ and $+10.9<\delta^{18}O<+17.1$), except two cherts, which have negative δ^{30}Si values, but high δ^{18}O (up to $+19.5‰$). The pronounced positive correlations between δ^{30}Si, δ^{18}O and SiO_2 imply that the isotope variation is driven by the silicification process which coevally introduced both ^{18}O and ^{30}Si into the basalts. The oxygen isotope variation in the basalts from about 8.6‰ to 15.6‰ is likely to represent temperature-dependent isotope fractionation during alteration. Our proposed model for the observed silicon isotope variation relies on a temperature-controlled basalt dissolution vs. silica deposition process.

© 2010 Elsevier B.V. All rights reserved.

1. Introduction

Processes in the hydrosphere of the Archaean Earth may have been very different from the present day. The ubiquity of cherts in 3.5–3.2 Ga greenstone belts shows that silica was extensively precipitated from seawater, probably due to the absence of silica-secreting organisms that maintained Archaean seawater close to silica saturation conditions (Siever, 1992; Treguer et al., 1995). In addition, pervasive silicification of submarine volcanic rocks appears to have been a characteristic feature prior to 3.0 Ga (e.g. Duchac and Hanor, 1987; Hanor and Duchac, 1990; Hofmann and Wilson, 2007). Silicification of volcanic and overlying sedimentary rocks and correlation of δ^{18}O values and SiO_2 contents have been interpreted by Hofmann and Harris (2008) to be a result of seafloor alteration by diffuse, low-temperature hydrothermal fluids, but both the source of silicon (Si) and the impact and magnitude of silicification processes in the early Archaean external silicon cycle remain unclear. Investigating the mechanisms of silica precipitation and silicification of volcanic rocks and seafloor sediments in the Eo- and Palaeoarchaean may provide insights not only into seawater–lithosphere interactions on the early Earth, but also into the role of seafloor hydrothermal activity for the chemical evolution of the early oceans. The mechanism of silica deposition is also relevant for the controversial suggestion that cherts are excellent preservation environments for early life on Earth (Pinti et al., 2009; Schopf, 1993), and possibly also on Mars (Farmer and Des Marais, 1999).

Si isotopes represent an important tool to check the role of the seawater percolation in the silicified Archaean lithosphere. Fluid-derived silica-rich precipitates (e.g. André et al., 2006; Basile-Doelsch et al., 2005; Ding et al., 1996; Robert and Chaussidon, 2006; van den Boorn et al., 2007, 2010) as well as secondary minerals formed by weathering (De La Rocha et al., 2000; Delstanche et al., 2009; Ding et al., 2004; Georg et al., 2006, 2007b; Opfergelt et al., 2009; Ziegler et al., 2005) are enriched in ^{28}Si, leading to a ^{28}Si depletion of their residual fluids. As a consequence, we should expect that gradual developments of ocean-derived Si-rich deposits would lead the ocean towards more positive δ^{30}Si signatures (Robert and Chaussidon, 2006). Mineral precipitation from such an isotopically fractionated ocean (residence time of Si $= 10^5$ yr; Siever, 1992), should therefore contrast with the rather limited range of δ^{30}Si variation in mafic and ultramafic igneous rocks ($\delta^{30}Si = -0.29 \pm 0.08‰$, Fitoussi et al., 2009; Georg et al., 2007a,b; Savage et al., 2010). In contrast, silica-rich minerals precipitating from a hydrothermal fluid equilibrated with basalt would have a very ^{28}Si-

* Corresponding author. Johannes Gutenberg—Universität Mainz, Institut für Geowissenschaften, Fachbereich 09, Becherweg 21, D-55099 Mainz, Germany. Tel.: +49 6131 3922295; fax: +49 6131 3923070.
E-mail address: abraha@uni-mainz.de (K. Abraham).

0012-821X/$ – see front matter © 2010 Elsevier B.V. All rights reserved.
doi:10.1016/j.epsl.2010.11.002

enriched component (δ^{30}Si < −0.29‰). Thus, Si isotopic ratios unravel the contributions of pure hydrothermal (δ^{30}Si ≪ −0.29‰), basaltic (δ^{30}Si ~ −0.29‰) and seawater-derived (δ^{30}Si ≫ −0.29‰) silica.

In addition, Si isotopes are resistant to metamorphic resetting (André et al., 2006; Robert and Chaussidon, 2006; van den Boorn et al., 2007, 2010). As Si concentrations are much lower than those of oxygen (O) in hydrothermal and metamorphic fluids, the Si isotope ratios of metamorphosed Archaean rocks are more likely to be close to their original magmatic values than oxygen isotopes. Robert and Chaussidon (2006) used the Si isotope variation in cherts as an indirect palaeotemperature indicator, based on the assumption that seafloor hydrothermal fluids, which precipitate a large fraction of their dissolved Si within altered oceanic crust, have variable δ^{30}Si values as a function of seawater temperature, resulting in corresponding variation in marine cherts. They observed an increase in δ^{30}Si values in cherts through time, which, together with a similar rise in chert δ^{18}O values over the same time span, they ascribed to a decrease in ocean temperatures from ~70 °C at 3.5 Ga to present day values. This interpretation was challenged by van den Boorn et al. (2010), who noted that primary and secondary cherts should be distinguished. Cherts that directly formed by chemical precipitation (C-cherts) show the largest spread in δ^{30}Si (−2.4‰ up to +0.6‰) and their isotopic signature reflects the degree of fractionation of hydrothermal fluids or the degree of mixing with seawater. In contrast, secondary cherts that developed by silicification of volcanogenic sediments (S-cherts) display a more restricted range of δ^{30}Si (+0.1‰ to +1.1‰), pointing to seawater as the dominant source of silica.

Combined O and Si isotope data give us further information about the mechanisms of silicification, because these isotope systems show opposite fractionation behaviour during the precipitation of silica, and the amount of oxygen in the fluid remains constant, in contrast to silicon.

We investigated three sections of variably silicified basalt and overlying chert from different stratigraphic units of the Onverwacht Group, Barberton Greenstone Belt (BGB), ranging in age from 3.54 to 3.33 Ga. All sections exhibit a gradual increase in the intensity of silicification within the basalt towards the capping chert. By comparing Si and O isotope variation in these sections, we are able to establish the controlling factors of isotope variation.

2. Geological background

The supracrustal succession of the BGB is situated in the eastern part of the Kaapvaal Craton in South Africa and Swaziland (Brandl et al., 2006; de Ronde and de Wit, 1994; Lowe and Byerly, 1999, 2007; Viljoen and Viljoen, 1969). The BGB can be divided into three main stratigraphic units; 1) the Onverwacht Group, a predominantly volcanic sequence, 2) the Fig Tree Group, a volcaniclastic and fine-grained siliciclastic succession and 3) the Moodies Group composed predominantly of sandstones (Lowe and Byerly, 1999, 2007). The Onverwacht Group formed between 3.55 and 3.30 Ga (Byerly et al., 1996; Kröner et al., 1996) and consists of submarine ultramafic and mafic volcanic rocks (komatiites, komatiitic basalts, basalts) and minor felsic (dacitic) volcanic rocks, which are intercalated with thin, silicified sedimentary units, deposited during breaks in volcanic activity. The stratigraphic thickness of the Onverwacht Group ranges from 1 km in the western and northern edge of the belt to more than 10 km in the southern part (Lowe and Byerly, 2007). It can be subdivided into six different units, the Sandspruit, Theespruit, Komati, Hooggenoeg, Kromberg and Mendon Formations. The metamorphic grade is mainly greenschist facies, but reaches amphibolite facies in the Sandspruit and Theespruit Formations (Lowe and Byerly, 1999).

We have investigated three sections of variably silicified rocks with overlying chert horizon from the: 1) Theespruit Formation, 2) Hooggenoeg Formation and 3) Kromberg Formation (GPS-coordinates of the sections are given in the Table 1). Silicification is accompanied by a change in the mineral assemblage. With increasing silicification, the paragenesis changes from an amphibole–garnet paragenesis (Theespruit Formation) or an epidote–chlorite paragenesis (Kromberg and Hooggenoeg Formations) to an assemblage dominated by quartz, carbonates and sericite. Detailed descriptions of these sections are provided in Hofmann and Bolhar (2007) and Hofmann and Harris (2008).

Table 1
Average δ^{30}Si-values of the chemical and analytical replicates and standard deviation ($2\sigma_{SD}$) in conjunction with SiO_2, depth and δ^{18}O. GPS-coordinates are given in brackets after the sample location.

Sample	Description	SiO_2 (%)	Depth (m)	δ^{18}O (‰)	Average δ^{30}Si (‰)	n	2 std. deviation (‰)a
Kromberg (S25°55.140′; E30°58.900′)							
AK15	Banded bl/w chert	96.4	2	15.4	0.55	2	0.09
AK12*	Sil. pb.	87.5	−0.7	15.3	0.81	2	0.02
AK4	Bl. chert-vein	97.9	−2	15.1	0.40	2	0.03
AK3*	Sil. pb.	84.8	−10	15.6	0.63	2	0.04
AK13	Bl. chert-vein	97.9	−12	16.2	0.40	2	0.13
AK2	Bl. chert, finely laminated	100.1	−29	19.5	−0.15	2	0.02
AK14	Banded bl/w chert	98.0	−25	16.5	−0.35	2	0.03
AK7*	Sil. pb.	84.8	−32	15.1	0.74	2	0.04
AK11*	Sil. pb.	81.2	−46	15.6	0.65	2	0.02
AK1*	Sil. pb.	76.8	−64	10.0	−0.22	2	0.06
AK10*	Unsil. pb.	51.9	−131	11.9	−0.21	3	0.07
Average							0.05
Hooggenoeg (S25°01.372′; E30°59.339′)							
H3B	Gr. chert (lapilli)	92.3	0.7	16.7	1.05	2	0.10
H2B	Bl. chert	97.1	0.5	17.0	0.80	2	0.05
AH14	Gr. chert (glass shards)	90.1	0.2	15.8	0.60	2	0.15
H1B	Bl. chert-vein	98.5	−1	17.1	0.48	3	0.11
AH15	Bl. chert-vein	98.9	−2	16.4	0.50	3	0.08
AH13*	Sil. pb.	70.3	−1.5	14.9	0.41	2	0.03
AH16	Sil. b.	76.3	−5	15.6	0.60	3	0.12
AH12*	Sil. mb.	74.8	−7	15.4	0.62	2	0.02
AH11*	Sil. pb.	73.4	−19	14.3	0.39	2	0.01
AH18*	Sil. pb. center	54.7	−30	12.2	−0.02	2	0.05
AH18R	Sil. pb. rim	46.6	−30	12.3	−0.07	2	0.10
AH10*	Unsil. pb. center	43.1	−60	9.0	−0.44	2	0.05
AH10R	Unsil. pb. rim	39.7	−60	8.6	−0.64	2	0.01
AH17*	Unsil. pb. center	50.9	−150	9.4	−0.24	3	0.12
AH17R	Unsil. pb. rim	53.1	−150	9.6	−0.41	2	0.08
Average							0.07
Theespruit (S25°59.917′; E30°50.092′)							
AT1*	Mafic schist, unsil. mb.	47.6	16	8.8	−0.06	2	0.07
AT2*	Felsic schist	76.3	12.5	10.9	0.29	2	0.14
AT3	Carb chert/shale	89.3	13	11.6	0.30	3	0.02
TS2	Carb shale	90.7	3	12.0	0.21	2	0.07
AT4*	Felsic schist	93.9	2	12.0	0.81	2	0.09
AT5R	Sil. pb., sheared	84.1	−1	11.9	0.39	4	0.12
AT5M*	Sil. pb., sheared	76.0	−1	11.9	0.46	2	0.07
AT6*	Sil. pb., sheared	58.9	−5	10.8	0.23	2	0.03
AT7*	Mafic schist, unsil. mb.	47.8	−18	9.9	−0.33	2	0.06
AT8*	Unsil. pb.	50.2	−30	10.4	−0.01	2	0.10
AT9*	Unsil. mb.	48.9	−55	8.9	−0.299	3	0.10
Average							0.08
Average all							0.07

Abbreviations: bl = black; w = white; sil = silicified; pb = pillow basalt; unsil = unsilicified, gr = green; b = basalt; mb = massive basalt. "*n*" stands for the number of chemical and analytical Si isotope replicates.
"a" denotes the standard deviation between the chemical and analytical replicates.
"R" stands for rim and "*" is labelling the samples described in Hofmann and Harris (2008).

2.1. Investigated samples and petrography

2.1.1. Theespruit Formation (3.55 Ga)

The Theespruit Formation is made up largely of metamorphosed komatiitic basalt, basalt, and sericitic and aluminous rocks representing

silicified felsic volcanic and volcaniclastic–epiclastic rocks. The felsic units are commonly associated with thin layers of carbonaceous chert. Theespruit felsic schists in the Steynsdorp Anticline have been dated at 3547 Ma by zircon $^{207}Pb/^{206}Pb$ evaporation (Kröner et al., 1996) and thus represent the oldest supracrustal rocks of the Barberton belt.

The section investigated for this study is from NE of Tjakastadt. It is composed of intercalated pillow and massive basalts, which are more strongly silicified towards the overlying felsic schist. The basalts contrast with those of the other two formations investigated in that they are more strongly foliated and more strongly metamorphosed, as garnet porphyroblasts are locally present in the silicified pillow basalts. Diener et al. (2005) reported *P–T* conditions of 7.4 ± 1.0 kbar and 560 ± 20 °C for rocks of this area. Overlying the basalts are siliceous felsic schists that are intercalated by discontinuous thin layers of carbonaceous chert. The felsic schists are strongly silicified cherty rocks that consist of silicified felsic agglomerates in low strain domains and, locally, conglomerates. Massive, unsilicified komatiitic basalt overlies the felsic schists.

2.1.2. Hooggenoeg Formation (3.45 Ga)

The Hooggenoeg Formation can be subdivided into several stratigraphic units (H2 to H5), denoted with "v" or "c", representing a volcanic interval (H2v–H5v) or a capping chert horizon (H2c–H5c), respectively (Lowe and Byerly, 1999). We investigated the uppermost section of basalt of the Hooggenoeg Formation from the east limb of the Onverwacht Anticline. Section H5 consists of a few hundred metres thick succession of undeformed variolitic pillow and massive basalts (H5v) that are silicified immediately below a thin horizon of strongly silicified sedimentary rock referred to as chert horizon H5c (Lowe and Byerly, 1999). A massive dacite unit (H6) has been dated by U–Pb in zircon at ca. 3.45 Ga (Armstrong et al., 1990; De Vries et al., 2006; de Wit et al., 1987). A network of black carbonaceous chert veins transects the uppermost 5 metres of the volcanic sequence. Remains of purported microfossils have been reported from one of these veins (Glikson et al., 2008). The contact between basalt and bedded chert is sharp and planar with no evidence of tectonic movement. The chert unit is about 1 m thick and consists of three different types of silicified sediments (from base to top): green chert (silicified vitric tuff with glass shards), massive black chert (silicified carbonaceous sediment) and green chert (silicified ash with accretionary lapilli).

2.1.3. Kromberg Formation (3.33 Ga)

The Kromberg Formation is well exposed on the west limb of the Onverwacht anticline, where it has been subdivided into three informal members (Lowe and Byerly, 1999), the Buck Reef Chert (K1), mafic lapilli tuff and lapillistone (K2) and tholeiitic basalt (K3). The section investigated for this work is situated in the central part of the BGB at the top of the Kromberg Formation (K3). A sequence of variably silicified pillow basalts is intercalated and capped by banded carbonaceous chert (K3c of Lowe and Byerly, 1999) that forms two laterally traceable horizons, the upper one, a tuffaceous band, which is 5 cm thick, contains igneous zircons with a mean age of $3334 + 3$ Ma (Byerly et al., 1996).

The volcanic succession consists of pillow basalt, of which the uppermost 50 m is silicified. The pillow basalt is locally slightly foliated and commonly variolitic. In the uppermost few meters of the section, translucent chert forms anastomosing veins and voids in pillows. Basalt is overlain by a black and white banded chert and a finely laminated black chert, representing the upper boundary of the first part of the section. Above this, there is a further zone of strongly silicified pillow and massive basalts and overlying black/white banded chert horizon. Hence two cycles of silicified basalts and overlying cherts were studied in the same section.

3. Analytical methods and chemical preparation techniques

Major and trace element as well as oxygen isotope data of most of the rocks are described in Hofmann and Harris (2008). In order to complete the data set, additional samples were investigated. Samples from Hofmann and Harris (2008) were re-analysed for major and trace elements (Table S1 in Supplementary information) for several reasons: 1) all rock powders were crushed at the University of Mainz by tungsten carbide instead of agate mills in order to avoid silicon contamination. 2) For Si isotope analysis, knowledge about the exact SiO_2 content is essential for the recovery-check during the dissolution steps and 3) in order to have a consistent data set.

3.1. Silicon isotopes

The samples were crushed using a tungsten-carbide pestle and mortar. Powder was dried in an oven overnight at 100 °C. About 5 mg of the rock powder were dissolved in a clean laboratory environment using alkaline attack ($LiBO_2$ flux, Abraham et al., 2008). Silicon was then purified by co-precipitation with triethylamine-molybdate (De La Rocha et al., 1996). The precipitate was then dried and combusted in Pt crucibles in a furnace at 1000 °C. The residue was a pure powder of cristobalite and tridymite (De La Rocha et al., 1996), which was transferred to polypropylene vials and dissolved in dilute Suprapur HF–HCl mixture.

We analysed silicon isotopes using a Nu Plasma™ MC-ICP-MS (Nu Instruments, Wrexham UK, Belshaw et al., 1998) at the Université Libre de Bruxelles (Belgium). Silicon isotopes are expressed by the conventional δ-notation in per mil (‰) deviation from a reference. Data are reported relative to in-house standards ($pSiO_2$ or Quartz Merck) which are isotopically similar (Abraham et al., 2008) to NBS28 (National Institute of Standard and Technology RM #8546), the reference standard for silicon isotopes (Carignan et al., 2004). Mass bias was corrected for by a standard-sample bracketing protocol, using external Mg doping in dynamic mode (Cardinal et al., 2003), but slightly modified to allow measurement of both $\delta^{30}Si$ and $\delta^{29}Si$ (Abraham et al., 2008). Accuracy of Si isotopic values was checked using the Diatomite standard, the composition of which has been established that was confirmed by an inter-laboratory comparison (Reynolds et al., 2007).

All $\delta^{30}Si$ and $\delta^{29}Si$ data fall along the mass-dependent terrestrial fractionation lines of Si ($R^2 = 0.98$, Fig. S1 in Supplementary information) describing either kinetic ($\delta^{29}Si = 0.5092 * \delta^{30}Si$) or equilibrium ($\delta^{29}Si = 0.5178 * \delta^{30}Si$) fractionations which are indistinguishable at such low degrees of fractionation (Young et al., 2002). This $\delta^{30}Si$–$\delta^{29}Si$ correlation demonstrates the quality of the isotopic determinations. The complete data set of $\delta^{30}Si$ is presented in Table 1 along with $\delta^{18}O$ and SiO_2 concentrations. All samples have been at least fully duplicated (including different aliquots, chemical separation and spectrometric determinations); they display an average reproducibility for $\delta^{30}Si$ of 0.07 ‰ ($2\sigma_{SD}$; SD = standard deviation, Table 1).

3.2. Oxygen isotopes

Oxygen isotopes were analysed at the University of Cape Town (UCT), South Africa and are expressed by the δ-notation in per mil (‰) deviation from SMOW. The NBS28 standard was analysed with every batch of samples and the raw data were normalized to the SMOW scale using the value of 9.64‰ for NBS28 recommended by Coplen et al. (1983). Based on the reproducibility of NBS28 analyses, the typical error on a $\delta^{18}O$ determination is ± 0.1‰ (1σ). Oxygen isotope compositions of silicate whole rocks were determined using conventional extraction methods after reaction with ClF_3 (Hofmann and Harris, 2008). The O_2 was converted to CO_2 using a hot platinised carbon rod. Isotope ratios were measured using a Finnigan MAT Delta XP mass spectrometer. Further details of the methods employed for the extraction of oxygen from silicates are given by Harris et al. (2000). The results of oxygen isotope analysis are reported in Table 1.

4. Results

4.1. Major and trace elements

The major and trace element data are presented in Table S1 of the supplementary material. The decrease with depth in SiO_2 content is the most significant change in major element concentrations below the capping cherts. The basalt sections show compositional changes typical for silicification as reported by Duchac and Hanor (1987) and Hofmann and Harris (2008).

4.2. Stable isotope variations

δ^{30}Si and δ^{18}O values are presented in Table 1 and in stratigraphic columns of the studied sections (Fig. 1). Our δ^{30}Si and δ^{18}O data are compared with those of terrestrial reservoirs.

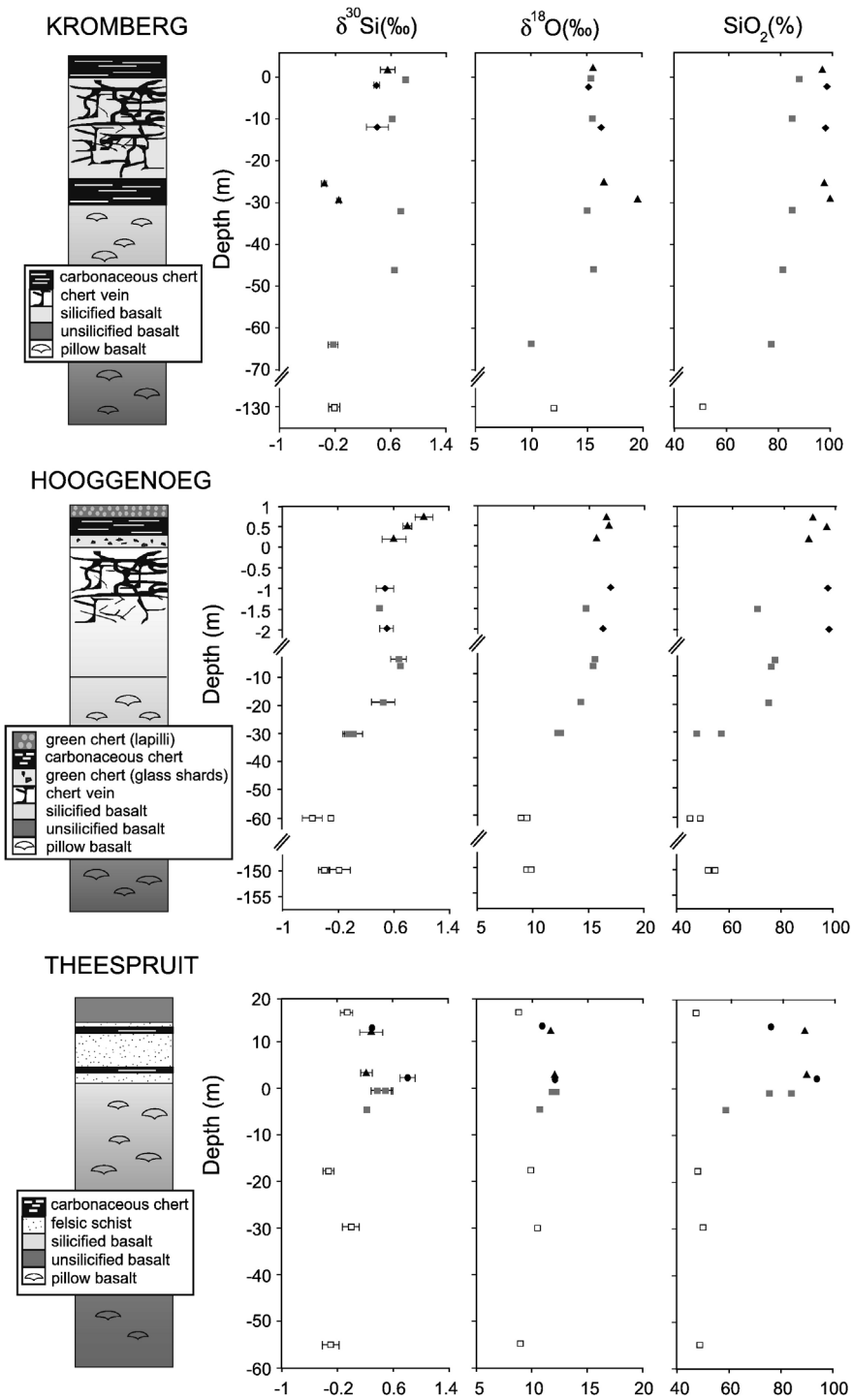

Fig. 1. δ^{30}Si and δ^{18}O values and SiO_2 plotted against stratigraphic height for the Kromberg, Hooggenoeg and Theespruit Formations. The image on the left shows the schematic stratigraphy of the sections investigated. Symbols refer to rock types: unsilicified basalts (open squares), silicified basalts (grey squares), cherts (black triangles), chert veins (black diamonds) and felsic schists (black circles). All sections show a change to higher δ^{30}Si and δ^{18}O with increasing grade of silicification (SiO_2 concentration). Error bar on δ^{30}Si represents the standard deviation between the replicates. Error bar of the oxygen isotopes characterize the standard error (~0.1‰) and are smaller than symbol size.

4.2.1. Silicon stable isotope variations

δ^{30}Si values of unsilicified basalts in all three formations (−0.64‰ to −0.01‰, mean = −0.29‰) are similar to those of recent basaltic rocks and peridotites and their mean (−0.29‰) falls close to estimates of the Bulk Silicate Earth (BSE) Si isotopic composition (δ^{30}Si = −0.28 ± 0.06‰, Fitoussi et al., 2009; δ^{30}Si = −0.29 ± 0.08‰, Savage et al., 2010). Compared to pillow centres, rims demonstrate no change in oxygen isotope composition but a systematic depletion in ^{30}Si (average Δ^{30}Si = +0.13‰), and variable SiO_2 contents but the two factors are not correlated and these enrichments may not be significant because they are close to, or within the analytical uncertainty. The δ^{30}Si values for silicified basalts (−0.22‰ to +0.81‰, mean = +0.40‰) change towards more positive values in all three sections with increasing grade of silicification (Figs. 1 and 2).

All but two cherts and all silicified felsic schists have ^{28}Si-depleted signatures (+0.21‰ to +1.05‰, mean = +0.53‰) and bear close resemblance to the Si isotope values of the silicified volcanogenic sediments (S-type cherts), which have been interpreted to contain silica derived from δ^{30}Si-enriched seawater (cf. van den Boorn et al., 2007, 2010). Additionally, chondritic Y/Ho ratios (~26), small Eu anomalies (0.8–2.8, average: 1.6) and high Al_2O_3 contents are typical for cherts formed by silicification of sedimentary or volcaniclastic material (Table S1 in supplementary material). The cherts have δ^{30}Si values in the middle of the range obtained by Robert and Chaussidon (2006) for Barberton cherts (−0.58‰ < δ^{30}Si < +1.95‰). However, the chert δ^{30}Si values are significantly higher than those in metacherts from Isua (−1.99‰ to −0.25‰, André et al., 2006) and cherts associated with Banded Iron Formations (BIFs; Ding et al., 1996; Steinhoefel et al., 2009). Two cherts with negative δ^{30}Si were found in the Kromberg Formation. This signature and their low Al_2O_3-contents point to a relatively pure chemical precipitate (C-type cherts; cf. van den Boorn et al., 2007, 2010; δ^{30}Si of −2.4‰ to +0.6‰) although they lack a positive Y/Ho anomaly characteristic for marine chemical precipitates (Bolhar et al., 2004). Vein cherts resemble isotopically silicified basalts (+0.48‰ < δ^{30}Si < +0.50), although they have much higher SiO_2 contents.

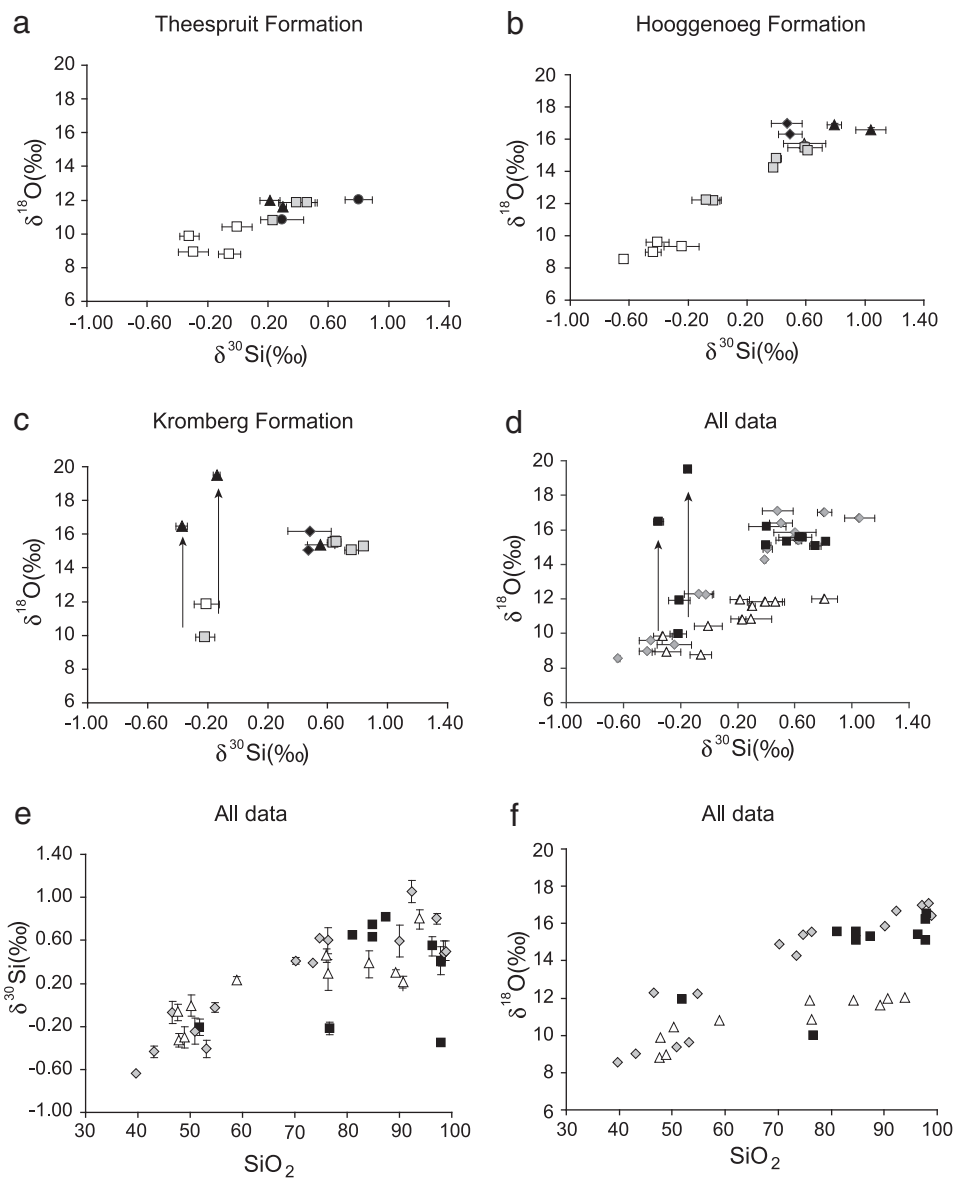

Fig. 2. (a,b,c) Plots of δ^{30}Si vs. δ^{18}O for the Theespruit, Hooggenoeg and Kromberg Formations, showing coupled behaviour of silicon and oxygen isotopes during the silicification process. For symbols see Fig. 1. Panels d, e and f show the complete data set of all three sections: (c,d) plots of δ^{30}Si vs. δ^{18}O: modelled water-rock interaction (Supplementary material: Calculation S1), is illustrated schematically by arrows facing upwards, since the computed results show only a change to higher δ^{18}O. (e) plots of SiO_2 vs. δ^{30}Si and (f) SiO_2 vs. δ^{18}O. Theespruit Formation is illustrated by white triangles, the Hooggenoeg Formation by grey diamonds and the Kromberg Formation by black squares.

4.2.2. Oxygen stable isotope variations

There is an increase in $\delta^{18}O$ value from unsilicified basalt (+8.6‰ to +11.9‰; mean = +9.6‰) to silicified basalt (+10.0‰ to +15.6‰; mean = +13.6‰), and to chert (+10.9‰ to +17.1‰; mean = +14.7‰). The unsilicified rocks have slightly higher $\delta^{18}O$ values than a suite of variably altered mafic and ultramafic samples from the Onverwacht Group (Hoffman et al., 1986; group B, +5.5‰ to +8.4‰). Isotopic studies of Archaean komatiites and their primary magmatic minerals from Quebec (Canada), Western Australia and the Barberton Greenstone Belt yielded $\delta^{18}O$ values that are not very different from those of modern mantle-derived mafic magmas ($\delta^{18}O$ = +5.6‰ to +6.0‰, Beaty and Taylor, 1982; Smith et al., 1984). The similarity indicates that the mantle source for Archaean komatiites had the same isotope composition. At the high degrees of partial melting necessary for the generation of Archaean tholeiites and komatiites (Arndt et al., 2009), the mantle can be regarded as an isotopically uniform reservoir of O. Therefore the $\delta^{18}O$ values of the unsilicifed basalts from this study are unlikely to be those of the original unaltered rock. $\delta^{18}O$ values of basalts increase, as do $\delta^{30}Si$ values, with increasing degree of silicification ($\delta^{18}O$ up to +15.6‰). The $\delta^{18}O$ values of chert veins (+16.4‰ to +17.1‰) and bedded cherts (+15.8‰ to +17.0‰) are similar to cherts from the Onverwacht Group previously analysed (+15.1‰ to +22.7‰, Robert, 1988; +9.4‰ to 22.7‰, Knauth and Lowe, 1978; +13.9‰ to +16.5‰, Robert and Chaussidon, 2006).

It is notable that there is a strong positive correlation between $\delta^{30}Si$ and $\delta^{18}O$ (Fig. 2a–d). Data arrays from the Kromberg and Hooggenoeg sections are similar. In contrast, the Theespruit data array has a different gradient in the $\delta^{30}Si$ vs. $\delta^{18}O$ plot. $\delta^{30}Si$ and $\delta^{18}O$ values generally correlate positively with SiO_2 in the Hooggenoeg and Theespruit Formations (Fig. 2e,f). Kromberg Formation data show more scatter due to the presence of two chert samples with negative $\delta^{30}Si$ values, but high $\delta^{18}O$.

5. Discussion

$\delta^{30}Si$ values of unsilicified basalts of this study resemble $\delta^{30}Si$ values of Phanerozoic basalts and are close to the Bulk Silicate Earth (BSE) value ($\delta^{30}Si = -0.28 \pm 0.06$‰, Fitoussi et al., 2009; $\delta^{30}Si = -0.29 \pm 0.08$‰, Savage et al., 2010). In contrast, the average $\delta^{18}O$ values of the unsilicified rocks (+9.6 ± 1.1‰) are significantly higher than fresh modern basalts and Archaean komatiites from Barberton, which have mantle-like $\delta^{18}O$ values ($\delta^{18}O$ = +5.6‰ to +6.0‰, Beaty and Taylor, 1982; Smith et al., 1984). This indicates that the pristine oxygen isotope composition of the basalts is not preserved even in the least silicified rocks. Smith et al. (1984) argued that an increase in $\delta^{18}O$ value of Barberton pillow lavas may have taken place shortly after emplacement of these lavas on the seafloor, prior to the onset of silicification, when rapid effusion of pillow lavas resulted in exchange processes with deep-seated water. In that case, the slightly higher $\delta^{18}O$ values of the unsilicified basalts are likely to be the result of these low-temperature alteration processes. In the present study we cannot determine whether or not this alteration is closely linked and coeval to the silicification. However in the following discussion we will compare the silicification to these unsilicified rocks, on the basis of the sound working hypothesis that the latter represent the altered protoliths on which the silicification was superimposed.

The pronounced positive correlations between $\delta^{30}Si$, $\delta^{18}O$ and SiO_2 (Fig. 2) imply that the variation in isotope composition for both O and Si is driven by the silicification process. This shows that silicification raised both $\delta^{18}O$ and $\delta^{30}Si$ in the altered basalts. There is a consensus (e.g. Hanor and Duchac, 1990; Hofmann and Harris, 2008) that pervasive silicification as recorded in strata from Barberton required the introduction of large volumes of Si-rich fluids that led to the breakdown of silicates in the basalts. Whatever the source of the fluid (seawater, transformed seawater, pure hydrothermal fluids), the fluid O/Si ratio must be very high, which means that the observed isotopic covariation cannot be the mere consequence of a fluid–rock exchange, even for very high fluid/rock ratio and near-saturation dissolved silicon content (see Supplementary information: Calculation S1). Water–rock interaction causes only a change to higher $\delta^{18}O$. Such a process may have led to the creation of the two cherts of the Kromberg formation with negative $\delta^{30}Si$, but high $\delta^{18}O$ (results of Calculation S1 of the water–rock interaction is shown as two arrows facing upwards in Fig. 2c,d).

Any proposed model has to meet the following constraints:

1) The precipitation process depends on the fraction of both elements remaining in the solution. The amount of oxygen in the fluid is so abundant that it should have remained constant during precipitation, so that the $\delta^{18}O$ of the water ought not to have changed through time at constant temperature. In contrast, considering the limited concentration of Si dissolved at saturation level (e.g., for a temperature range of $T = 0$ to 200 °C the solubility of quartz and amorphous silicon would be between 2.4 ppm and 132 ppm and 31.5 ppm and 441 ppm, respectively; Gunnarsson and Arnórsson, 2000).
2) Due to the effectively constant amount of oxygen in the fluid during precipitation, the oxygen isotope fractionation between a silica precipitate and the fluid is mostly temperature dependent (Clayton et al., 1972; Matsuhisa et al., 1979). Therefore the oxygen isotope variation in the basalts from about 8.6‰ to 15.6‰ is likely to represent a temperature-dependent isotope fractionation during alteration. Due to the inverse relationship of the temperature and fractionation factor, the downwards decreasing oxygen isotope composition is likely to hint at a downwards increase in temperature. As the silicification of the basalts leads to an higher $\delta^{18}O$ value than the value of modern mantle-derived mafic magmas ($\delta^{18}O$ = +5.6‰ to +6.0‰, Beaty and Taylor, 1982; Smith et al., 1984), low-temperature conditions (in the range of 100 °C to 150 °C) for the silicification process are assumed (Gregory and Taylor, 1981).
3) Both isotope systems yield opposite fractionation factors for silica precipitation. Precipitated silica will have a $\delta^{18}O$ value that is higher than the fluid from which it formed, because $\Delta^{18}O_{qtz-water}$ is always positive (e.g. Matsuhisa et al., 1979). In contrast, silica-rich precipitates have lower $\delta^{30}Si$ ratios than the dissolved Si in the fluid (e.g. André et al., 2006; Basile-Doelsch et al., 2005; Ding et al., 1996; Georg et al., 2009; Steinhoefel et al., 2010) with a probable water–silica mass fractionation factor of about −2.3‰ (Delvigne et al., 2010; Van den Boorn et al., 2010). At constant temperature, irrespective of the initial isotopic composition of the fluid, the $\delta^{30}Si$ in both residual solutions and successive precipitates will therefore quickly increase during progressive precipitation. An increase in temperature downwards, should theoretically lead to a decrease of Si isotope fractionation factors at equilibrium conditions between phases (Méheut et al., 2007, 2009). This would certainly lessen the $\delta^{30}Si$ increase in both residual solutions and successive precipitates, but would not significantly modify the trend for precipitates to quickly move to higher $\delta^{30}Si$ values downwards.

From these constraints, it is obvious that both the silicon and oxygen isotope systems should show an antithetic behaviour during single-stage silica precipitation from a fluid with less positive signature for O and more positive isotopic composition for Si. This is strictly at variance with the observed positive covariation between the two isotopic systems. Therefore, we have to invoke a two-step process to explain the data.

A likely scenario is the change of silicon solubility within a temperature gradient downwards in the section (Fig. 3). In the upper colder alteration zone the solution should be oversaturated in silica resulting in extensive silica precipitation and rapid exhaustion of silicon from the solution, with residual solutions quickly moving to heavier Si isotopic signatures. In parallel, the downward temperature

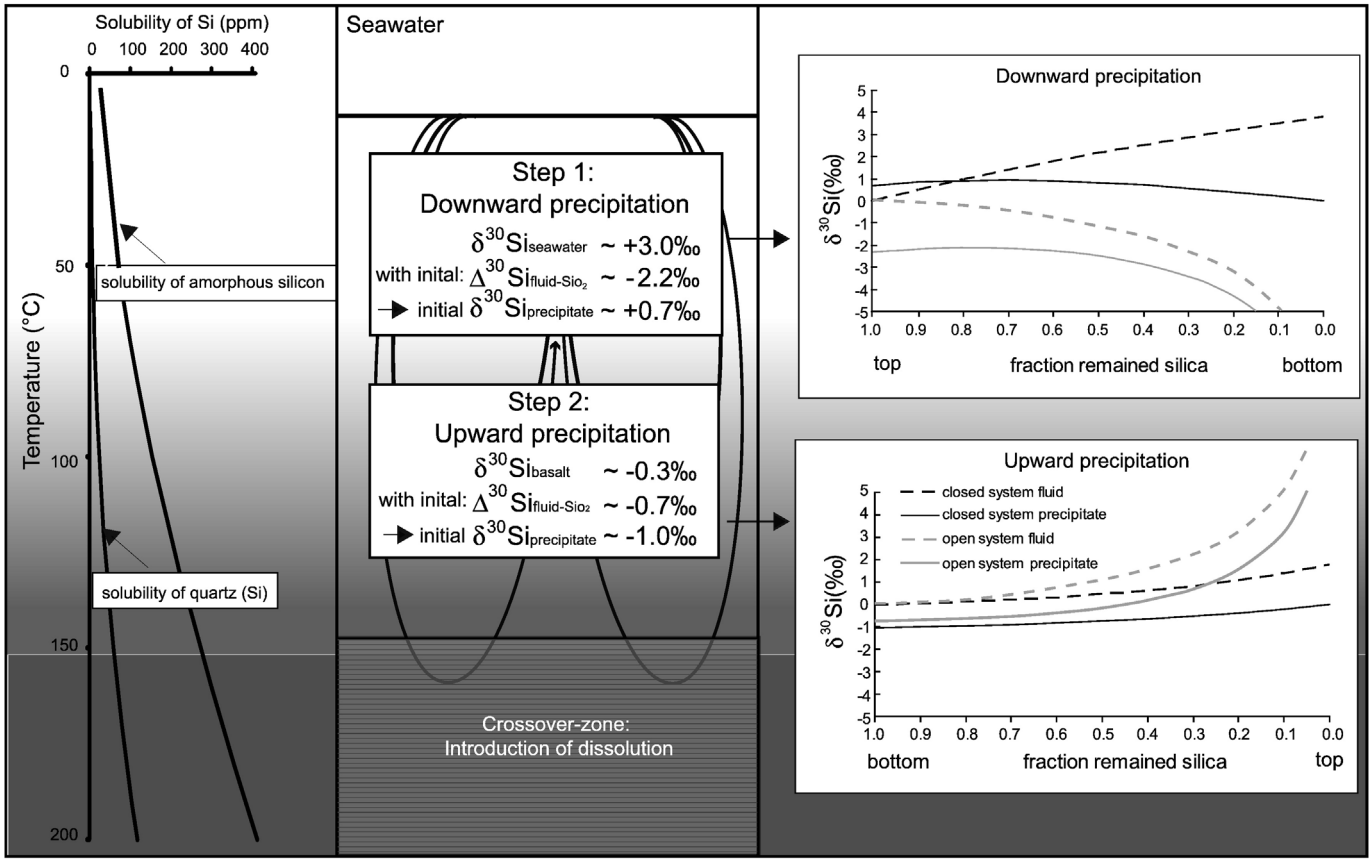

Fig. 3. Model of temperature-controlled basalt dissolution and silica deposition. Oxygen isotopes yield information about the temperature conditions (low-temperature alteration at top of the section and increasing temperature towards the bottom) during the precipitation of silica, O is compared to Si not depending on the fraction of remaining silica. The silicon isotope composition requires at a two-step precipitation process involving different solubility conditions in a convecting fluid. Temperature-dependent silicon solubility curves (0° to 200 °C) of quartz and amorphous silicon are illustrated on the left hand side. Silicon contents were calculated using the temperature-dependent solubility (K) equations of Gunnarsson and Arnórsson (2000), (cf., Robert and Chaussidon, 2006). Temperature-dependent silicon isotope fractionation models with different initial isotope compositions are shown on the right hand side (Supplementary material: Calculation S2). The input parameters for the calculation (initial isotope composition and fractionation factors) of downward and upward-moving fluids are illustrated as step1 and step 2, respectively in the boxes in the middle. At the top of the section, the fluid is close to saturation and thus the amount of precipitated silica is high, whereas the opposite is true at the bottom. Fractionation models (Supplementary material: Calculation S2) show that the downward-moving fluid evolves to lower Si isotope composition due to the change in fractionation factor with temperature. Owing to high solubility at the bottom of the section there is a crossover-zone, where the dissolution of the basalt is introduced and precipitation stops. Therefore, the upward percolating fluid adopts the isotopic value of the basalt and gradually deposits a silica-rich fraction with a much lighter isotopic composition (δ^{30}Si ~ −1.0‰) which evolves to higher δ^{30}Si values with advancing precipitation.

increase must have rapidly enhanced the saturation concentration level. As a consequence, there will be a crossover point at a distinct level in the section, where precipitation stops and the dissolution of the basalts starts (Gunnarsson and Arnórsson, 2000). This will lead to a gradual recharge of the fluid with basalt-derived lighter Si close to a BSE-like Si isotopic composition of δ^{30}Si = −0.3‰. On its way back to the surface within a convection cell, such a fluid will cool down, gradually depositing a silica-rich fraction with an isotopic composition much lighter than its initial Si isotopic composition (≪−0.3 ‰). This will evolve to higher δ^{30}Si values with advanced precipitation, overprinting the more positive signature precipitated on the way down. To sum up, mixed downward and upward-moving Si-rich fluid fluxes will give rise to a mixture of low-T heavy silica derived from the seawater on the top of the silicified zone and higher-T light silica derived from the rock dissolution. This two-step model gives a basic explanation for the positive correlation between δ^{30}Si and δ^{18}O despite the antithetic isotopic fractionation behaviour of silicon and oxygen during silica precipitation.

The wholesale precipitation of silica from seawater in the first step of downward percolation should influence the isotope composition of seawater. The composition of Archaean seawater is poorly constrained, but was likely close to silica saturation with regard to amorphous silica (Siever, 1992), so that silica precipitation occurred relatively easily during any perturbation such as a drop in temperature (Posth et al., 2008). Any precipitation of amorphous silica from such a reservoir would tend to move the δ^{30}Si of the residual dissolved silicon to higher values with time (Robert and Chaussidon, 2006). The increase in Si isotopic value from the Theespruit (+0.21‰ < δ^{30}Si < +0.81‰) to the Hooggenoeg/Kromberg cherts (+0.40‰ < δ^{30}Si < +1.05‰) fit such a trend of increasing δ^{30}Si of seawater from 3.54 Ga to 3.45–3.33 Ga. From this positive signature, assuming a water–silica fractionation factor of Δ^{30}Si$_{water-silica}$ ~ −2.3‰ (Delvigne et al., 2010; Van den Boorn et al., 2010), and a one-step silica–seawater isotopic fractionation between these cherts and the silicifying seawater, it could be inferred that the seawater δ^{30}Si was close to +3‰ in the early Archaean.

Recent Si isotopic investigations of BIFs, and chemically-precipitated cherts (André et al., 2006; Delvigne et al., 2010; Ding et al., 1996; Steinhoefel et al., 2009, 2010; Van den Boorn et al., 2007, 2010) have demonstrated that most of these seawater-derived deposits bear a rather negative Si isotopic signature (average δ^{30}Si = −1.74 ± 0.63 1 std for n = 40) whatever their age in the 3.8–2.9 Ga time interval. We deliberately ignore here the more positive isotopic signature of the cherts analysed by Robert and Chaussidon (2006), because we cannot be sure whether they represent chemically-precipitated cherts or silicified tuffs. Considering a water–silica fractionation factor of Δ^{30}Si$_{water-silica}$ ~ −2.3‰ (Delvigne et al., 2010; Van den Boorn et al., 2010), this imposes that the oceanic reservoir has been kept at a slightly positive signature (δ^{30}Si ~ +0.5‰) during a large time span

during the Archaean and not at +3‰ as proposed above. To maintain the oceanic reservoir in such a steady-state despite extensive precipitation of light silica in BIFs and cherts, Steinhoefel et al. (2010) proposed to balance the low δ^{30}Si outputs by a high δ^{30}Si sink reservoir. The widespread silicification of Early Archaean volcanic rocks on the seafloor might represent this missing complementary reservoir.

6. Conclusions

The combined Si and O isotope data reported here provide a new perspective on early Archaean chert formation and related silicification processes as well as providing some new key parameters to monitor the chemical evolution of the Precambrian oceans and to constrain better the silica-rich environments in which early fossils have been discovered.

Silicification introduces high δ^{18}O and δ^{30}Si values into the precursor rocks, which is at variance with an antithetic isotope fractionation behaviour of both isotope systems. The oxygen isotope composition depends only on temperature owing to buffering by the high and effectively constant amount of oxygen in the fluid during precipitation. In contrast, the silicon isotope composition is controlled by the opposite effects of the downward and upward vertical migration of fluids that vary in their initial isotope composition and in fractionation factors: the different temperature at their sources causes different solubilities and consequently counteracting isotope signatures on precipitation.

The high δ^{30}Si values of the silicified volcanic rocks raise the possibility that they might represent the complementary reservoir to the low δ^{30}Si values in BIFs and cherts.

Supplementary materials related to this article can be found online at doi:10.1016/j.epsl.2010.11.002.

Acknowledgements

KA is supported by the “Deutsche Forschungsgemeinschaft” and DC by the Belgian Science Policy. AH acknowledges support by NRF grant FA2007043000008. LA thanks BELSPO for several financial supports in the SPSD programs. We are grateful to S. Opfergelt, A. Heuser, L. Monin, N. Dahkani, N. Mattielli and J.T.M. de Jong for technical and scientific support, and Antje Huttenlocher and Nora Groschopf for major and trace element analyses on the XRF. Friedhelm von Blanckenburg and an anonymous reviewer are thanked for their constructive criticisms on the manuscript. R.W. Carlson is thanked for the editorial handling and helpful comments.

References

Abraham, K., Opfergelt, S., Fripiat, F., Cavagna, A.J., de Jong, J.T.M., Foley, S.F., André, L., Cardinal, D., 2008. δ^{30}Si and δ^{29}Si determinations on USGS BHVO-1 and BHVO-2 reference materials with a new configuration on a Nu plasma multi-collector ICP-MS. Geostand. Geoanal. Res. 32, 193–202.

André, L., Cardinal, D., Alleman, L.Y., Moorbath, S., 2006. Silicon isotopes in 3.8 Ga West Greenland rocks as clues to the Eoarchean supracrustal Si cycle. Earth Planet. Sci. Lett. 245, 162–173.

Armstrong, R.A., Compston, W., de Wit, M.J., Williams, I.S., 1990. The stratigraphy of the 3.5–3.2 Ga Barberton Greenstone Belt revisited: a single zircon ion microprobe study. Earth Planet. Sci. Lett. 101, 90–106.

Arndt, N.T., Coltice, N., Helmstaedt, H., Gregoire, M., 2009. Origin of Archean subcontinental lithospheric mantle: some petrological constraints. Lithos 109, 61–71.

Basile-Doelsch, I., Meunier, J.D., Parron, C., 2005. Another continental pool in the terrestrial silicon cycle. Nature 433, 399–402.

Beaty, D.W., Taylor, H.P., 1982. Some petrologic and oxygen isotopic relationships in the Amulet Mine, Noranda, Quebec, and their bearing on the origin of Archean massive sulfide deposits. J. Econ. Geol. 77, 95–108.

Belshaw, N.S., Freedman, P.A., O'Nions, R.K., Frank, M., Guo, Y., 1998. A new variable dispersion double-focusing plasma mass spectrometer with performance illustrated for Pb isotopes. Int. J. Mass Spectrom. 181, 51–58.

Bolhar, R., Kamber, B.S., Moorbath, S., Fedo, C.M., Whitehouse, M.J., 2004. Characterisation of early Archaean chemical sediments by trace element signatures. Earth Planet. Sci. Lett. 222, 43–60.

Brandl, G., Cloete, M., Anhaeusser, C.R., 2006. Archean greenstone belts. In: Johnson, M.R., Anhaeusser, C.R., Thomas, R.J. (Eds.), The Geology of South Africa. Geological Society of South Africa. Johannesburg/Council for Geoscience, Pretoria, pp. 9–56.

Byerly, G.R., Kröner, A., Lowe, D.R., Todt, W., Walsh, M.M., 1996. Prolonged magmatism and time constraints for sediment deposition in the early Archaean Barberton Greenstone Belt: evidence from the Upper Onverwacht and Fig Tree Groups. Precambrian Res. 78, 125–138.

Cardinal, D., Alleman, L.Y., de Jong, J., Ziegler, K., André, L., 2003. Isotopic composition of silicon measured by multicollector plasma source mass spectrometry in dry plasma mode. J. Anal. Atom. Spectrom. 18, 213–218.

Carignan, J., Cardinal, D., Eisenhauer, A., Galy, A., Rehkämper, M., Wombacher, F., Vigier, N., 2004. A reflection on Mg, Cd, Ca, Li and Si isotopic measurements and related reference materials. Geostand. Geoanal. Res. 28, 139–148.

Clayton, R.N., O'Neil, J.R., Mayeda, T.K., 1972. Oxygen isotope exchange between quartz and water. J. Geophys. Res. 77, 3057–3067.

Coplen, T.B., Kendall, C., Hopple, J., 1983. Comparison of stable isotope reference samples. Nature 302, 236–238.

De La Rocha, C.L., Brzezinski, M.A., DeNiro, M.J., 1996. Purification, recovery, and laser-driven fluorination of silicon from dissolved and particulate silica for the measurement of natural stable isotope abundances. Anal. Chem. 68, 3746–3750.

De La Rocha, C.L., Brzezinski, M.A., DeNiro, M., 2000. A first look at the distribution of stable isotopes of silicon in natural waters. Geochim. Cosmochim. Acta 64, 2467–2477.

de Ronde, C.E.J., de Wit, M.J., 1994. Tectonic history of the Barberton Greenstone Belt, South Africa: 490 million years of Archean crustal evolution. Tectonics 13, 983–1005.

De Vries, S.T., Nijman, W., Armstrong, R.A., 2006. Growth-fault structure and stratigraphic architecture of the Buck Ridge volcano-sedimentary complex, upper Hooggenoeg Formation, Barberton Greenstone Belt, South Africa. Precambrian Res. 149, 77–98.

de Wit, M.J., Armstrong, R., Hart, R.J., Wilson, A.H., 1987. Felsic igneous rocks within the 3.3–3.5 Ga Barberton Greenstone Belt: high crustal level equivalents to the surrounding tonalite–trondhjemite terrain, emplaced during thrusting. Tectonics 6, 529–549.

Delstanche, S., Opfergelt, S., Cardinal, D., Elsass, F., André, L., Delvaux, B., 2009. Silicon isotopic fractionation during adsorption of aqueous monosilicic acid onto iron oxide. Geochim. Cosmochim. Acta 73, 923–934.

Delvigne, C., Cardinal, D., Hofmann, A., André, L., 2010. Combining Ge/Si ratios and Si isotopes to constraint the origin of a mesoarchean banded iron formation. Extended abstract. 5th International Archean Symposium, Perth, Western Australia.

Diener, J.F.A., Stevens, G., Kisters, A.F.M., Poujol, M., 2005. Metamorphism and exhumation of the basal parts of the Barberton Greenstone Belt, South Africa: constraining the rates of Mesoarchaean tectonism. Precambrian Res. 143, 87–122.

Ding, T., Jiang, S., Wan, D., Li, Y., Li, J., Song, H., Liu, Z., Yao, X., 1996. Silicon Isotope Geochemistry. Geological Publishing House, Beijing, China.

Ding, T., Wan, D., Wang, C., Zhang, F., 2004. Silicon isotope compositions of dissolved silicon and suspended matter in the Yangtze River, China. Geochim. Cosmochim. Acta 68, 205–216.

Duchac, K.C., Hanor, J.S., 1987. Origin and timing of metasomatic silicification of an early Archean komatiite sequence, Barberton Mountain Land, South Africa. Precambrian Res. 37, 125–146.

Farmer, J.D., Des Marais, D.J., 1999. Exploring for a record of ancient Martian life. J. Geophys. Res. 104, 26977–26995.

Fitoussi, C., Bourdon, B., Kleine, T., Oberli, F., Reynolds, B.C., 2009. Si isotope systematics of meteorites and terrestrial peridotites: implications for Mg/Si fractionation in the solar nebula and for Si in the Earth's core. Earth Planet. Sci. Lett. 287, 77–85.

Georg, R.B., Reynolds, B.C., Frank, M., Halliday, A.N., 2006. Mechanisms controlling the silicon isotopic composition of river waters. Earth Planet. Sci. Lett. 249, 290–306.

Georg, R.B., Halliday, A.N., Schauble, E.A., Reynolds, B.C., 2007a. Silicon in the Earth's core. Nature 447, 1102–1106.

Georg, R.B., Reynolds, B.C., West, A.J., Burton, K.W., Halliday, A.N., 2007b. Silicon isotope variations accompanying basalt weathering in Iceland. Earth Planet. Sci. Lett. 261, 476–490.

Georg, R.B., Zhu, B., Reynolds, B.C., Halliday, A.N., 2009. Stable silicon isotopes of groundwater, feldspars, and clay coatings in the Navajo Sandstone aquifer, Black Mesa, Arizona, USA. Geochim. Cosmochim. Acta 73, 2229–2241.

Glikson, M., Duck, L.J., Golding, S., Hofmann, A., Bolhar, R., Webb, R., Baiano, J., Sly, L., 2008. Microbial remains in some earliest Earth rocks: comparison with a potential modern analogue. Precambrian Res. 164, 187–200.

Gregory, R.T., Taylor, H.P., 1981. An oxygen isotope profile in a section of Cretaceous oceanic crust, Samail ophiolite, Oman: evidence for δ^{18}O buffering of the oceans by deep (N5 km) seawater-hydrothermal circulation at mid-ocean ridges. J. Geophys. Res. 86, 2737–2755.

Gunnarsson, I., Arnórsson, S., 2000. Amorphous silica solubility and the thermodynamic properties of $H_4SiO_4^\circ$ in the range of 0° to 350 °C at P_{sat}. Geochim. Cosmochim. Acta 64, 2295–2307.

Hanor, J.S., Duchac, K.C., 1990. Isovolumetric silicification of early Archean komatiites: geochemical mass balances and constraints on origin. J. Geol. 98, 863–877.

Harris, C., Smith, S., le Roex, A.P., 2000. Oxygen isotope composition of phenocrysts from Tristan da Cunha a Gough Island lavas: variation with fractional crystallisation and evidence for assimilation. Contrib. Mineral. Petrol. 138, 164–175.

Hoffman, S.E., Wilson, M., Stakes, D.S., 1986. Inferred oxygen isotope profile of Archaean oceanic crust, Onverwacht Group, South Africa. Nature 321, 55–58.

Hofmann, A., Bolhar, R., 2007. The origin of carbonaceous cherts in the Barberton Greenstone Belt and their significance for the study of early life in mid-Archaean rocks. Astrobiology 7, 355–388.

Hofmann, A., Harris, C., 2008. Silica alteration zones in the Barberton Greenstone Belt: a window into subseafloor processes 3.5–3.3 Ga ago. Chem. Geol. 257, 221–239.
Hofmann, A., Wilson, A.H., 2007. Silicified basalts, bedded cherts and other sea floor alteration phenomena of the 3.4 Ga Nondweni greenstone belt, South Africa. In: Van Kranendonk, M.J., Smithies, R.H., Bennett, V. (Eds.), Earth's oldest rocks: Developments in Precambrian Geology, 15, pp. 571–605.
Knauth, L.P., Lowe, D.R., 1978. Oxygen isotope geochemistry of cherts from the Onverwacht Group (3.4 billion years), Transvaal, South Africa, with implications for secular variations in the isotopic composition of cherts. Earth Planet. Sci. Lett. 41, 209–222.
Kröner, A., Hegner, E., Wendt, J.I., Byerly, G.R., 1996. The oldest part of the Barberton granitoid–greenstone terrain, South Africa: evidence for crust formation between 3.5 and 3.7 Ga. Precambrian Res. 78, 105–124.
Lowe, D.R., Byerly, G.R., 1999. Stratigraphy of the west-central part of the Barberton Greenstone Belt, South Africa. In: Lowe, D.R., Byerly, G.R. (Eds.), Geologic Evolution of the Barberton Greenstone Belt, South Africa. Geological Society of America Special Paper, 329. Geological Society of America, Boulder, CO, pp. 1–36.
Lowe, D.R., Byerly, G.R., 2007. An overview of the geology of the Barberton Greenstone Belt and vicinity: implications for early crustal development. In: Van Kranendonk, M.J., Smithies, R.H., Bennett, V.C. (Eds.), Earth's Oldest Rocks. Developments in Precambrian Geology, 15. Elsevier, Amsterdam, pp. 481–526.
Matsuhisa, Y., Goldsmith, J.R., Clayton, R.N., 1979. Oxygen isotopic fractionation in the system quartz–albite–anorthite–water. Geochim. Cosmochim. Acta 43, 1131–1140.
Méheut, M., Lazzeri, M., Balan, E., Mauri, F., 2007. Equilibrium isotopic fractionation in the kaolinite, quartz, water system: prediction from first-principles density-functional theory. Geochim. Cosmochim. Acta 71, 3170–3181.
Méheut, M., Lazzeri, M., Balan, E., Mauri, F., 2009. Structural control over equilibrium silicon and oxygen isotopic fractionation: a first-principles density-functional theory study. Chem. Geol. 258, 28–37.
Opfergelt, S., de Bournonville, G., Cardinal, D., André, L., Delstanche, S., Delvaux, B., 2009. Impact of soil weathering degree on silicon isotopic fractionation during adsorption onto iron oxides in basaltic ash soils, Cameroon. Geochim. Cosmochim. Acta 73, 7226–7240.
Pinti, D.L., Mineau, R., Clement, V., 2009. Hydrothermal alteration and microfossil artefacts of the 3,465-million-year-old Apex chert. Nat. Geosci. 2, 640–643.
Posth, N.R., Hegler, F., Konhauser, K.O., Kappler, A., 2008. Alternating Si and Fe deposition caused by temperature fluctuations in Precambrian oceans. Nat. Geosci. 1, 703–708.
Reynolds, B.C., Aggarwal, J., André, L., Baxter, D., Beucher, C., Brzezinski, M.A., Engström, E., Georg, B., Land, M., Leng, M.J., Opfergelt, S., Rodushkin, I., Sloane, H.J., van den Boorn, S.H.J.M., Vroon, P.Z., Cardinal, D., 2007. An inter-laboratory comparison of Si isotope reference materials. J. Anal. Atom. Spectrom. 22, 561–568.
Robert, F., 1988. Carbon and oxygen isotope variations in Precambrian cherts. Geochim. Cosmochim. Acta 52, 1473–1478.
Robert, F., Chaussidon, M., 2006. A palaeotemperature curve for the Precambrian oceans based on silicon isotopes in cherts. Nature 443, 969–972.
Savage, P.S, Georg, R.B., Armytage, R.M.G., Williams H.M., Halliday, A.N., 2010. Silicon isotope homogeneity in the mantle. Earth Planet. Sci. Lett. 295, 139–146.
Schopf, J.W., 1993. Microfossils of the early Archean Apex chert: new evidence of the antiquity of life. Science 260, 640–646.
Siever, R., 1992. The silica cycle in the Precambrian. Geochim. Cosmochim. Acta 56, 3265–3272.
Smith, H.S., O'Neil, J.R., Erlank, A.J., 1984. Oxygen isotope compositions of minerals and rocks and chemical alteration patterns in pillow lavas from the Barberton Greenstone Belt, South Africa. In: Kröner, A. (Ed.), Archaean Geochemistry. Springer, pp. 115–137.
Steinhoefel, G., Horn, I., von Blanckenburg, F., 2009. Micro-scale tracing of Fe and Si isotope signatures in banded iron formation using femtosecond laser ablation. Geochim. Cosmochim. Acta 73, 5343–5360.
Steinhoefel, G., von Blanckenburg, F., Horn, I., Konhauser, K.O., Beukes, N.J., Gutzmer, J., 2010. Deciphering formation processes of banded iron formations from the Transvaal and the Hamersley successions by combined Si and Fe isotope analysis using UV femtosecond laser ablation. Geochim. Cosmochim. Acta 74, 2677–2696.
Treguer, P., Nelson, D.M., Van Bennekom, A.J., DeMaster, D.J., Leynaert, A., Queguiner, B., 1995. The silica balance in the world ocean: a reestimate. Science 268, 375–379.
Van den Boorn, S.H.J.M., van Bergen, M.J., Nijman, W., Vroon, P.Z., 2007. Dual role of seawater and hydrothermal fluids in Early Archean chert formation: evidence from silicon isotopes. Geology 35, 939–942.
Van den Boorn, S.H.J.M., van Bergen, M.J., Vroon, P.Z., de Vries, S.T., Nijman, W., 2010. Silicon isotope and trace element constraints on the origin of ~3.5 Ga cherts: implications for early Archaean marine environments. Geochim. Cosmochim. Acta 74, 1077–1103.
Viljoen, M.J., Viljoen, R.P., 1969. An introduction to the geology of the Barberton granite–greenstone terrain. Spec. Publ. Geol. Soc. S. Afr. 2, 9–28.
Young, E.D., Galy, A., Nagahara, H., 2002. Kinetic and equilibrium mass-dependent isotope fractionation laws in nature and their geochemical and cosmochemical significance. Geochim. Cosmochim. Acta 66, 1095–1104.
Ziegler, K., Chadwick, O.A., Brzezinski, M.A., Kelly, E.F., 2005. Natural variations of δ^{30}Si ratios during progressive basalt weathering, Hawaiian Islands. Geochim. Cosmochim. Acta 69, 4597–4610.